Iterative Reconstruction for PET scanners with continuous scintillators

Ana Iriarte[1], Gabriel Caffarena[1], Mariano López-Fernández[1], Rodrigo García-Carmona[1], Abraham Otero[1], Carlos O.S. Sorzano[1,2] and Roberto Marabini[3]

***Abstract*— Several technical developments have led to a comeback of the continuous scintillators in positron emission tomography (PET). Important differences exist between the resurgent continuous scintillators and the prevailing pixelated devices, which can translate into certain advantages of the former over the latter. However, if the peculiarities of the continuous scintillators are not considered in the iterative reconstruction in which the measured data is converted to images, these advantages will not be fully exploited. In this paper, we review which those peculiarities are and how they have been considered in the literature of PET reconstruction. In light of this review, we propose a new method to compute one of the key elements of the iterative schemes, the system matrix. Specifically, we substitute the traditional Gaussian approach to the so-called uncertainty term by a more general Monte Carlo estimation, and account for the effect of the optical photons, which cannot be neglected in continuous-scintillators devices. Finally, we gather in a single scheme all the elements of the iterative reconstruction that have been individually reformulated, in this or previous works, for continuous scintillators, providing the first reconstruction framework fully adapted to this type of detectors. The preliminary images obtained for a commercially available PET scanner show the benefits of adjusting the reconstruction to the nature of the scintillators.**

I. Introduction

The use of continuous scintillators instead of pixelated arrays as gamma photon detectors in Positron Emission Tomography (PET) provides higher sensitivity and spatial and energy resolution at lower cost and complexity [1],[2]. The continuous scintillators were introduced as PET detectors in 1990 [3]. The disadvantages associated to the use of thallium-doped sodium iodide Nai(TI) (needed to produce high light output), resulted in most of the groups abandoning the use of continuous detectors in favor of discrete configurations [4]. However, the advent of new materials along with other technical developments in the PET detection systems [4], have led to a renewed interest in continuous scintillators [5], [4], [6]. The reconstruction step, in which a mathematical algorithm converts the data provided by a PET camera to tomographic images, plays a key role in the PET studies. The most popular reconstruction schemes, the so-called iterative algorithms, use detailed models of the PET detection process. Although researchers have lately resumed the use of continuous sctintillators, their specific features have not yet been adequately incorporated to the iterative algorithms.

*Work supported by CEU San Pablo University under grant PPC12/2014.

[1]Ana Iriarte, Gabriel Caffarena, Mariano Fernandez Rodrigo G. Carmona and Abraham Otero are with CEU San Pablo University, 28668 Madrid, Spain ana.iriarte.ruiz@gmail.com

[2] Carlos O.S. Sorzano is with National Center of Biotechnology (CSIC), 28049 Madrid, Spain coss@cnb.csic.es

[3] Roberto Marabini is with Escuela Politécnica Superior, Universidad Autónoma de Madrid, 28049 Madrid, Spain roberto@cnb.csic.es

II. Objectives and Structure

This work provides a framework for the reconstruction of continuous scintillators PET data. First, in sections III and VI we introduce the two issues that should be considered in the reconstruction for continuous scintillators and review how these issues have been considered in the literature. Then, we propose measures to overcome the two weak points that have been found in previous approaches. In Section V we show how to improve the computation of the uncertainty term of the system matrix. In Section VI, we show how to incorporate the effect of the optical photons to the model. The implementation of the proposed measures is illustrated in Section VII for a commercial scanner. A continuous scintillators dedicated reconstruction scheme is used to obtain and evaluate images in Section VIII.

III. LORs Definition in Continuous Scintillators

The first difference that continuous scintillators introduce with respect to their pixelated counterparts is the definition of the so-called lines of response (LORs), that join the detector positions in which the two gamma photons resulting from the characteristic PET positron-electron annihilation are located. In pixelated designs, a LOR d is a tube defined by two discrete detectors (c_1 and c_2 in Figure 1(a)). In continuous scintillators, the tube reduces to a line defined by two continuous positions in the detectors (p_1 and p_2 in Figure 1(b)). The list-mode versions of the iterative algorithms [7] modify the traditional equations for LORs binned in discrete detectors to consider each LOR individually, and permit to retain the full precision of the continuous-defined LORs. But the continuous nature of the LORs involves other considerations. The iterative algorithms use the so-called system matrix, whose terms $p(b,d)$ stand for the probability that a positron emitted within a basis function b is detected at a LOR d. Most of the existing methodologies computes the system matrix terms as discrete probabilities of detection in a LOR. [8] and [9] consider the possible continuous nature of the scintillators and reformulate the discrete probabilities as likelihood values of a continuous probability distribution. They compute the system matrix through an integral scheme that models the geometry of the gamma pairs emission, the penetration of the photons in the detectors, and what is referred to as "uncertainty in the detection" and expressed as $p(d|d')$. This term stands for the likelihood that a coincidence taking place in a LOR d', is positioned in a different LOR

978-1-4244-9270-1/15/$31.00 ©2015 IEEE

d, with both LORs defined in a continuous domain. For the two first effects, well-established models are used: a uniform distribution of the emission directions, and an exponential distribution for the length the photon crosses the scintillator before interacting with it. For the uncertainty in the detection, in the absence of an accepted model, a Gaussian distribution is chosen. However, the Gaussian behavior of the uncertainty has been neither demonstrated nor guaranteed. The mispositioning of the coincidences arises from complex phenomena (mainly multiple Compton interactions) and depends on factors (detector dimensions, materials and configurations) that vary largely among the different devices. A more specific modeling for the $p(d|d')$ terms should thus be imposed. The reformulation of the system matrix for continuous-defined LORs also affects to the so-called sensitivity matrix, whose terms $p(b,.)$ stand for the probability that a pair of gamma photons emitted from a basis function b are detected. This probability has traditionally been computed as a discrete summation over the probabilities of detection in each LOR, but alternative methods for its computation for continuous scintillators have been developed (see [9] and the references therein).

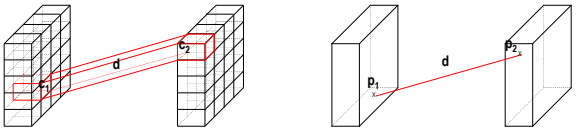

(a) (b)

Fig. 1. Definition of LORs in pixelated (a) and continuous (b) scintillators.

IV. Optical photons in Continuous Scintillators

The formal differences that the use of continuous scintillators make in the iterative reconstruction have been tackled so far. However, the use of continuous scintillators also makes important differences in the physical detection process, which concern the behavior of the optical photons that result from each of the interactions associated to a gamma photon. In pixelated detectors, these photons are confined to one optically isolated array and the light response properties are approximately identical regardless of the point within the segmented array from which the optical photons are emitted. However, in the continuous scintillators, the optical photons can propagate all over the continuous block and the shape of the light response function (LRF) can vary dramatically depending on the light source position. First, the LRF varies with the tangential 2D position on the crystal. For light sources close to the crystal side edges the reflecting light from the side surfaces contributes to the width and tail of the LRF (Figure 2a). The LRF changes as well with the depth of the light source within the crystal due to reflections from the top and back surfaces. Specifically, the LRF is less spread out for positions close to the detection system (Figure 2b). The distortions in the shape of the LRF degrade the intrinsic spatial resolution of continuous detector devices. Although these distortions have been partially compensated during the detector manufacturing process [4],[10],[11],[12], no work has been found in which these techniques are complemented with the inclusion of the optical photons behavior in the system model. This is likely due to the fact that the pixelated scintillators, where the LRF is not such an important issue, have been the most popular technology in the past decades.

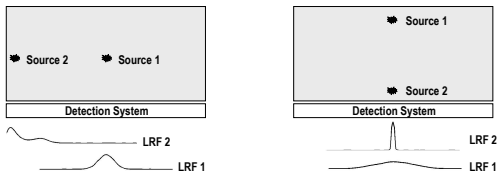

(a) (b)

Fig. 2. Approximated LRFs in a continuous scintillator.

V. Computation of the Uncertainty Term

We propose to substitute the Gaussian approximation ([8], [9]) by a device-specific estimation of the $p(d|d')$ terms using the GATE Monte Carlo (MC) simulator [13]. A MC estimation of analogous uncertainty terms for pixelated detectors is followed in [14] by simulating a coincidence in a discrete LOR d' a statistically reasonable number of times and histogramming the recorded positions in the discrete LOR positions d of the device. The resulting histograms, normalized for area 1, result in a collection of discrete distributions that are stored to be used at reconstruction time. We suggest to modify this procedure for continuous-defined LORs. First, we restate the discrete probability distributions as continuous distributions, substituting the histogramming by a smoothing normal kernel-based estimation [15], followed by a careful discretization of the resulting distributions. Details on this procedure are given in Section VII.

VI. Incorporation of the Optical Photons Effect

A gamma photon can undergo multiple interactions in the scintillator, each of which becomes a source of optical photons. Analytical models for these light sources exist [16],[17], but incorporating them to the system matrix is a great challenge. One light distribution has to be modeled for each interaction, which requires a foresight of the complex and unpredictable pattern of multiple interactions associated to each photon. Alternatively, we propose to use the GATE capabilities (which are usually switched off when simulating pixelated detectors) to generate and track optical photons. In Section VII we show how the simulation of the optical photons during the estimation of the uncertainty terms permits the inclusion of their effect in a very advantageous way.

VII. Implementation

This section illustrates the MC estimation of the uncertainty terms $p(d|d')$ for the Albira PET scanner [6]. The process of characterizing the materials and surfaces of the scintillations before the simulations (two factors that

strongly determine the behavior of optical photons) is a complex problem out of the scope of this work and thus a typical configuration [10] has been chosen. In order to remove possible mismatches between the simulated and the real data acquisition process, the evaluation of the new approach will be carried on just with reconstructions from data simulated with the same parameters used to obtain the system model. Although it would be interesting to study possible mismatches with real data, it is out of the scope of this paper and is left as future work. The estimation of the uncertainty terms $p(d|d')$ as continuous density functions is performed in two steps. First, the distributions are obtained with a very fine sampling of d' and d. In other words, a high number of distributions (corresponding to a high number of simulated LORs d') containing a large number of positions d are obtained. In the second step, the oversampled distributions are studied to perform a decimation of the d and d' variables consistent with a proper sampling. Using a large number of points improves the reliability of the study, and does not pose a problem of storage, since rapid RAM access to data is not needed before the reconstructions, and the distributions can be stored in disk at this point.

A. MC Estimation of the $p(d|d')$ distributions

We assume that, as in [8] and [9], $p(d|d')$ can be split as $p(d|d') = p(p_1|p'_1)p(p_2|p'_2)$, p'_1, p'_2 and p_1, p_2 being the pairs of points defining d' and d (as in Figure 1). In this way, the estimation of $p(d|d')$ reduces to the computation of $p(p|p')$, which stands for the probability that a photon interacting at a position p' is positioned at p. A collection of $p(p|p')$ has been obtained, corresponding to the simulation of p's at different depths and tangential positions in the scintillator. This permits accounting for the effect of the LRF variation along these dimensions, which, as previoulsy stated, is remarkable in continuous scintillators. Moreover, as in [14], the angular dimension is considered (i.e for each p', different angular orientations of the incident photon have been simulated). Switching on the optical capabilities of GATE increases considerably the simulation time (seven weeks for this work), but these simulations are run just once and for all before the reconstructions. Figures 3a, b and c show a illustrative sample of the distributions obtained using the MC simulations and the normal kernel smoother for different depths (z being the depth of interaction), tangential positions (x being the tangential distance to the crystal center) and orientations (gamma being the angular deviation from the normal incidence), respectively. δx stands for the location where each event is positioned. For the sake of space, just one of the two tangential dimensions and one of the angular dimensions are considered (the components located in the transaxial plane, but the results apply to the axial components). As can be observed, the distributions get narrower as p' gets closer to the detection system. Moreover, important distortions are appreciated in the shape of the distributions as p' is closer to the detector edge. Both observations are in accordance with the change in shape in the LRFs shown in Figure 2. However, no remarkable differences among the distributions due to the photon orientation are appreciated. The Lilliefors's test (used to check the hypothesis that data come from a normally distributed population) has been run for the positions recorded in each of the experiments. For the border distributions, the result indicates that the hypothesis can be rejected at a significance 5% level.

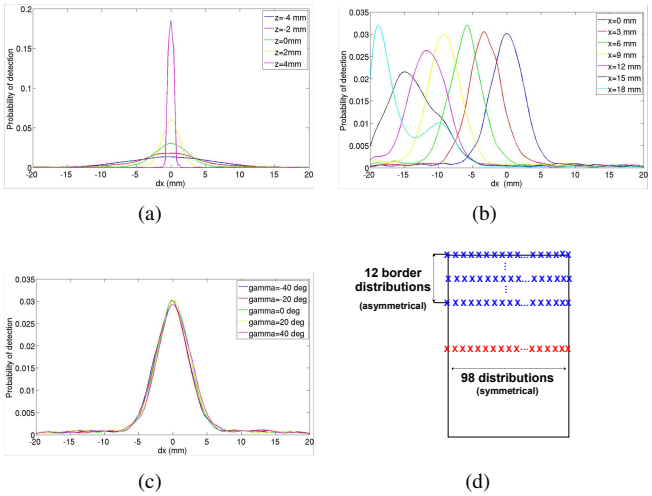

Fig. 3. $p(p|p')$ distributions for different depths (a), tangential positions (b) and incidence angles (c). Layout of p' in a detector (not to scale) (d).

B. Discretization of the $p(p|p')$ distributions

First, it has been determined the number of distributions to be stored (i.e the discretization of p'). As suggested by Figures 3a,b,c, the variability of the distributions with the position of p' has to be considered, but the incidence angle can be ignored. The distributions for p's at the central tangential position (red crosses in Figure 3) can be applied, by simple translation, to positions close to the center, but 12 specific distributions have to be used as p' approaches the side border (blue crosses in Figure 3). This number has been obtained measuring the distance between probability densities with the Kullback-Leibler (KL) divergence. The minimum separation among distributions has been chosen so that the KL among consecutive distributions is above a threshold, which has been computed using the well-known emission-distance independence [18] of the distributions (i.e by comparing the distributions obtained for photons with same interacting position and incidence angle but generated at different distances from the scintillator). As for the depth, using the same procedure the minimum separation between p's has been estimated to be $0.1mm$ for the total detector thickness of $9.8mm$. This gives place to $98(1+12) = 1,274$ total $p(p|p')$ distributions (which rotated apply to the axial dimension). Second, an effort has been made to maximize the precision with which p is sampled, in agreement with the objective of retaining as much as possible the continuous nature of the positioning. A thorough study of the distributions reveals that a sampling value of $\delta p = 0.2mm$ is accurate enough. In each distribution, p covers a range of $40mm$ (the tangential dimension), but for the 98 central symmetric

distributions just half of the points have to be stored. With these number of distributions and points by distribution, a total number of $245,000$ values have to be allocated, which fit easily in the current RAM of standard computers. This avoids costly disk access during the reconstructions and thus do not compromise the reconstruction time.

VIII. Reconstructions

The system and sensitivity matrix computed as in [9] have been incorporated to a list-mode reconstruction algorithm. In order to evaluate the improvements introduced, the uncertainty term of the system matrix has been implemented using three approaches. First, the terms $p(d|d')$ have been estimated as described in Section VII and will be referred to as $p_{REF}(d|d')$. Second, in order to evaluate if adapting the MC approach of [14] from pixelated to continuous crystals (using the kernel smoothing and subsequent thoughtful discretization) has any benefit, the distributions have been estimated as normalized histograms, with d' and d discretized in 1 mm steps (the average size of discrete crystals) and will be referred to as $p_{LOR}(d|d')$. Finally, it will be checked if modeling the optical photons has any effect on the reconstructions. As can be observed in Figure 3, the changing LRFs resulting from the complex reflection patterns of the scintillation light, translate into important differences in the shape of the uncertainty distributions. In order to check if taking into account these differences is worth, the third approach uses a single invariant distribution (corresponding to the center of the crystal) which will be referred to as $p_{INV}(d|d')$. Two sets of phantom activity distributions for the Albira scanner have been simulated with GATE. First, with the purpose of measuring the resolution, $800,000$ coincidences from a data set of point sources at the central transaxial plane in different radial positions facing the scintillators center has been generated. Second, in order to study the levels of noise amplification, $5,000,000$ coincidences from a unicorm cylinder have been obtained. Figures 4a,b and c show the radial, tangential, and axial resolution (as measured by FWHM) of the reconstructed points after 20 iterations. Figure 4d shows the image roughness (IR) (which measures the pixel to pixel variability in the image) vs the number of iterations of the reconstructed cylindrical phantom. As can be observed, the use of a kernel smoothing followed by a careful discretization of the $p(d|d')$ terms increases the resolution while reducing the noise propagation of the images compared with the histogramming of events. On the other hand, a significant improvement in the resolution of the reconstructions is achieved with the incorporation of the optical phenomena, with lower noise levels.

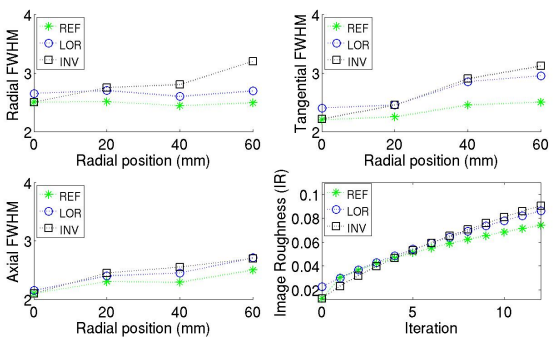

Fig. 4. Radial, tangential and axial FWHM against radial position of the point sources and Image roughness against iteration number of the cylinder.

Acknowledgment

We thank the use of resources at the Supercomputing Center of Galicia (CESGA).

References

[1] G. Llosa, R. Battiston, M. Bisogni *et al.*, "Novel silicon photomultipliers for PET application," in *Nuclear Science Symposium Conference Record, IEEE*, vol. 3, 2006, pp. 1875 –1879.

[2] P. Mendes, P. Bruyndonckx, J. Navarrete *et al.*, "Evaluation of monolithic detector blocks for high- sensitivity PET imaging of the human brain," in *Nuclear Science Symposium Conference Record, IEEE*, vol. 4, 2007, pp. 2953–2955.

[3] J. S. Karp, G. Muehllehner, D. A. MankofF *et al.*, "Continuous-slice PENN-PET: a positron tomograph with volume imaging capability." *J. Nuclear Medicine*, vol. 31, pp. 617–627, 1990.

[4] J. Benlloch, V. Carrilero, J. Catret *et al.*, "Design and calibration of a small animal PET scanner based on continuous LYSO crystals and PSPMTs," in *Nuclear Science Symposium Conference Record, IEEE*, vol. 4, 2006, pp. 2328–2332.

[5] S. Tavernier, P. Bruyndonckx, S. Leonard *et al.*, "A high-resolution PET detector based on continuous scintillators," *Nucl. Instrum. Methods Phys. Res., A*, vol. 537, pp. 321–325, 2005.

[6] F. Sánchez, L. Moliner, C. Correcher *et al.*, "Small animal PET scanner based on monolithic LYSO crystals: Performance evaluation." *Med Phys*, vol. 39, p. 643, 2012.

[7] A. J. Reader, R. Manavaki, S. Zhao *et al.*, "Accelerated list-mode EM algorithm," *Nuclear Science, IEEE Transactions on*, vol. 49, pp. 42–49, 2002.

[8] S. Staelens, Y. D'Asseler, S. Vandenberghe *et al.*, "A three-dimensional theoretical model incorporating spatial detection uncertainty in continuous detector PET." *Phys Med Biol*, vol. 49, pp. 2337–2350, 2004.

[9] A. Iriarte, C. O. S. Sorzano, J. M. Carazo *et al.*, "A theoretical model for em-ml reconstruction algorithms applied to rotating PET scanners." *Phys Med Biol*, vol. 54, pp. 1909–1934, 2009.

[10] E. Giménez, J. Benlloch, M. Gimenez *et al.*, "Detector optimization of a small animal PET camera based on continuous LSO crystals and flat panel PS-PMTs," in *Nuclear Science Symposium Conference Record, IEEE*, vol. 6, 2004, pp. 3885–3889.

[11] R. S. Miyaoka, S.-K. Joo, and K. Lee, "Detector light response modeling for a thick continuous slab detector." *J Nucl Sci Technol*, vol. 45, pp. 634–638, 2008.

[12] C. Lerche, A. Ros, J. M. Monzo *et al.*, "Maximum likelihood positioning for gamma-ray imaging detectors with depth of interaction measurement," *Nucl. Instrum. Methods Phys. Res., A*, vol. 604, pp. 359–362, 2009.

[13] S. Jan, G. Santin, D. Strul *et al.*, "GATE: a simulation toolkit for PET and SPECT," *Phys Med Biol*, vol. 49, pp. 4543–4561, 2004.

[14] S. Moehrs, M. Defrise, N. Belcari *et al.*, "Multi-ray-based system matrix generation for 3D PET reconstruction." *Phys Med Biol*, vol. 53, pp. 6925–6945, 2008.

[15] A. W. Bowman and A. Azzalini, *Applied Smoothing Techniques for Data Analysis: The Kernel Approach with S-Plus Illustrations (Oxford Statistical Science Series)*. Oxford University Press, USA, Nov. 1997.

[16] M. Aykac, H. Li, J. Uribe *et al.*, "A study of coincidence line spread function (CLSF) estimation for small scintillators using quadrant sharing technique," *Nuclear Science, IEEE Transactions on*, vol. 50, pp. 1331 – 1338, 2003.

[17] C. Levin, *Application-Specific Small Field-of-View Nuclear Emission Imagers in Medicine*, M. N. Wernick and J. N. Aarsvold, Eds. Academic Press, 2004.

[18] J. Qi, R. M. Leahy, S. R. Cherry *et al.*, "High-resolution 3D Bayesian image reconstruction using the microPET small-animal scanner," *Phys Med Biol*, vol. 43, pp. 1001–1013, 1998.